The following publication Jinhui Yuan, Zhe Kang, Feng Li, Xianting Zhang, Chao Mei, Guiyao Zhou, Xinzhu Sang, Qiang Wu, Binbin Yan, Xian Zhou, Kangping Zhong, Kuiru Wang, Chongxiu Yu, Gerald Farrell, Chao Lu, Hwa Yaw Tam, and P. K. A. Wai, "Experimental generation of discrete ultraviolet wavelength by cascaded intermodal four-wave mixing in a multimode photonic crystal fiber," Opt. Lett. 42, 3537-3540 (2017) is available at https://doi.org/10.1364/OL.42.003537.

Experimental generation of discrete ultraviolet wavelength by cascaded intermodal four-wave mixing in a multimode photonic crystal fiber

JINHUI YUAN,[1,2,†] ZHE KANG,[2,†,*] FENG LI,[2,†,*] XIANTING ZHANG,[2] CHAO MEI,[1] GUIYAO ZHOU,[3] XINZHU SANG,[1] QIANG WU,[4] BINBIN YAN,[1] XIAN ZHOU,[2] KANGPING ZHONG,[2] KUIRU WANG,[1] CHONGXIU YU,[1] GERALD FARRELL,[5] CHAO LU,[2] HWA YAW TAM,[6] AND P. K. A. WAI[2]

[1]*State Key Laboratory of Information Photonics and Optical Communications (Beijing University of Posts and Telecommunications), P.O. Box163 (BUPT), 100876 Beijing, China*

[2]*Photonics Research Centre, Department of Electronic and Information Engineering, The Hong Kong Polytechnic University, Hung Hom, Hong Kong*

[3]*Guangdong Provincial Key Laboratory of Nanophotonic Functional Materials and Devices, South China Normal University, 510006 Guangzhou, China*

[4]*Department of Physics and Electrical Engineering, Northumbria University, Newcastle upon Tyne, NE1 8ST, United Kingdom*

[5]*Photonics Research Centre, Dublin Institute of Technology, Dublin, Ireland*

[6]*Photonics Research Centre, Department of Electrical Engineering, The Hong Kong Polytechnic University, Hung Hom, Hong Kong*

[†]*These authors contributed equally to this work.*

[*]*Corresponding authors: zhe.kang@polyu.edu.hk, and enlf@polyu.edu.hk*

Received XX Month XXXX; revisedXX Month, XXXX; accepted XX MonthXXXX; posted XX Month XXXX (Doc. ID XXXXX); published XX Month XXXX

Intermodal four-wave mixing (FWM) in multimode optical fibers can be exploited to convert the available laser pump energy to the desired spectral regions. In this letter, we demonstrated experimentally for the first time discrete ultraviolet (UV) wavelength generation by cascaded intermodal FWM when femtosecond pump pulses at 800 nm are launched into the deeply normal dispersion region of the fundamental guided-mode of a multimode photonic crystal fiber (MPCF). For pump pulses at average input powers P_{av}=450, 550, and 650 mW, the first anti-Stokes waves are generated at the visible wavelength of 538.1 nm through intermodal phase-matching between the fundamental and second-order guided-mode of the MPCF. The first anti-Stokes waves generated then serve as the secondary pump for the next intermodal FWM process. The second anti-Stokes waves in the form of the third-order guided-mode are generated at the UV wavelength of 375.8 nm. The maximum output power is above 10 mW for P_{av}=650 mW. We also confirm that the influences of fiber bending and intermodal walk-offs on the cascaded intermodal FWM-based frequency conversion process are negligible.

OCIS codes: *(060.5295) Photonic crystal fibers; (190.4370) Nonlinear optics, fibers. (190.4380) Nonlinear optics, four-wave mixing*

http://dx.doi.org/10.1364/OL.99.099999

Spatially coherent ultraviolet (UV) light has important applications in biomedical science and fluorescence spectroscopy. At present, it remains difficult to generate discrete new wavelengths in the UV region from the available laser sources, which are centered at near-infrared wavelengths of 1550, 1064, and 800 nm. Although soliton-based generation of UV higher-order harmonics and resonant blue-shifted dispersive-wave radiations in the gases-filled hollow-core photonic crystal fibers (HC-PCFs) have already been reported [1], the conversion efficiencies of the pump wave to the UV wavelengths are very low. In addition, HC-PCFs are difficult to fabricate in practice, and the complex optical properties of the different gases used have to be considered.

Recently, multimode nonlinear fibers have been attracting much interest [2-6]. When ultrashort pulses are propagated inside a multimode optical fiber or PCF, nonlinear spatiotemporal effects, such as multimode soliton dynamics [7,8], intermodal modulation instability [9], intermodal four-wave mixing (FWM) [10-13], etc., could be triggered by controlling the guided-mode intercoupling and intermodal dispersion characteristics. Among the new nonlinear effects, intermodal FWM is a promising process for nonlinear frequency conversion. Compared with intramodal FWM, the phase-matching condition of intermodal FWM does not depend on the zero-dispersion wavelengths (ZDWs) of the optical fiber or PCF used. Thus, there are fewer constraints on the fiber design and the choice of the pump laser for such nonlinear optical process. Moreover, intermodal FWM can avoid the interference induced by the ZDW-dependent supercontinuum (SC) generation, and allows for the efficient conversion of the pump energy to the desired spectral regions, along with frequency shift of hundreds of THz relative to the initial pump wave. Intermodal FWM has been utilized to generate visible light down to green and blue wavelengths by near-infrared pumping [10-13]. To the best of our knowledge, there is no report of UV wavelength generation based on intermodal FWM.

In this letter, we have experimentally generated discrete UV wavelength for the first time by cascaded intermodal FWM in a multimode PCF (MPCF). When femtosecond pump pulses at 800 nm are launched into the deeply normal dispersion region of the fundamental guided-mode of the MPCF, the first anti-Stokes waves propagating as the second-order guided-mode are generated at 538.1 nm. They then serve as the secondary pump for the next intermodal FWM process. The second anti-Stokes waves are generated at 375.8 nm and propagated as the third-order guided-mode. We have also investigated the influences of fiber bending and intermodal walk-offs on the cascaded intermodal FWM process.

We use a solid-core air-silica MPCF designed and fabricated in our laboratory. Fig. 1(a) shows the cross-section image of the MPCF. The non-uniformity of the air-holes in the cladding region is mainly induced by the fluctuations of the gas pressure and fusion temperature during the fabrication process. The measured core diameter (D) and

average relative air-hole size (d/Λ) are 6.4 μm and ~0.89, respectively. Although this MPCF could support multiple guided-modes because of the large effective refractive index contrast between the silica-core and air-silica cladding, we focus on the characteristics of the fundamental (1st), second-order (2nd), and third-order (3rd) guided-modes in this work. We calculate the effective refractive indices of the 1st, 2nd, and 3rd guided-modes in the wavelength range from 0.3 to 2 μm, as shown in Fig. 1(b). Fig. 1(c) shows the group-velocity dispersion curves of the three guided-modes derived from the effective refractive indices in Fig. 1(b). From Fig. 1(c), the ZDWs of the 1st, 2nd, and 3rd guided-modes are 1074, 980, and 883 nm, respectively. The spatial distribution profiles of the three guided-modes calculated at 800, 538, and 376 nm are shown in insets 1, 2, and 3 of Fig. 1(c), respectively. In addition, from Fig. 1(c) the pump wavelength at 800 nm used in the experiment is far away from the ZDWs of the considered guided-modes of the MPCF, and lies in the deeply normal dispersion regions. Thus, instead of the ZDW-dependent intramodal FWM, intermodal FWM between the three guided-modes could take place.

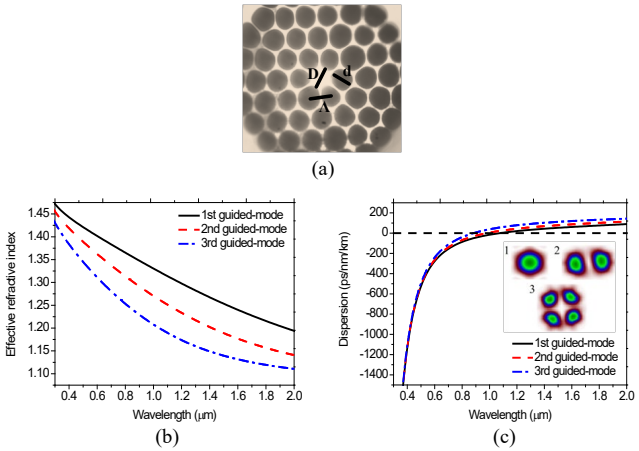

Fig. 1. (a) The cross-section image of the MPCF used. (b) The effective refractive index curves calculated for the fundamental (1st), second-order (2nd), and third-order (3rd) guided-modes of the MPCF. (c) The group-velocity dispersion curves of the three guided-modes derived from (b). Insets 1, 2, and 3 show the spatial distributions of the 1st, 2nd, and 3rd guided-modes calculated at wavelengths 800, 538, and 376 nm, respectively.

Fig. 2 shows the experimental set-up. We use a mode-locked Ti:sapphire laser centered at 800 nm as the pump source, which produces a femtosecond pulse train with duration 120 fs and repetition rate 76 MHz. In order to prevent the backscattered light from entering the laser cavity, an optical isolator is placed after the pump laser. With a grating-based compressor, a positive-chirp is introduced deliberately. The initial pump pulses are broadened from 120 to 273 fs. We also use a variable attenuator to adjust the average input powers. By using a 40× microscope objective, the stretched pump pulses are coupled into the 25-cm long MPCF. By monitoring and adjusting the coupling of the incident pump light with a black-and-white CCD camera, a free-space to fiber coupling efficiency of 65% is achieved. The CCD camera is also used to observe the far-field distributions of the initial pump and generated anti-Stokes waves from the output end of the MPCF. First, we adjust the injection conditions (incident angle relative to the fiber longitudinal axis and excitation radial position) to control the number of guided-modes propagating inside the MPCF and to ensure that the pump energy is coupled mainly into the 1st guided-mode of the MPCF. The fiber propagation loss is measured to be ~0.83 dB/m at 800 nm by the cut-back method. Two optical spectrum analyzers (OSA1 and OSA2) are used to record the output optical spectra after the other 40× microscope objective. The wavelength ranges of OSA1 and OSA2 are from 200 to 1100 nm and 900 to 2500 nm, respectively. The corresponding wavelength resolutions are 0.025 and 15 nm, respectively.

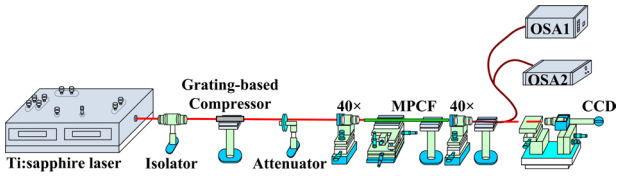

Fig. 2. The experimental set-up.

In cascaded intermodal FWM with degenerate pump configuration, two pump photons are coupled into the 1st guided-mode. The first anti-Stokes and Stokes photons, both propagating in the 2nd guided-mode, are simultaneously generated. Then, the first anti-Stokes photons serve as the secondary pump to generate the second anti-Stokes and Stokes photons, both propagating in the 3rd guided-mode. To determine the frequency conversion wavelengths, we calculate the intermodal phase-matching conditions without taking into account nonlinear contribution [11,12,14]. Thus, for the first and second intermodal FWM processes, intermodal phase-mismatch parameters $\delta\beta_{12}$ and $\delta\beta_{23}$ are given by $\delta\beta_{12}=2\beta^{(1)}(\omega_P)-\beta^{(2)}(\omega_{AS1})-\beta^{(2)}(\omega_{S1})$ and $\delta\beta_{23}=2\beta^{(2)}(\omega_{AS1})-\beta^{(3)}(\omega_{AS2})-\beta^{(3)}(\omega_{S2})$, where $\beta^{(1)}(\omega_P)$, $\beta^{(2)}(\omega_{AS1})$, and $\beta^{(2)}(\omega_{S1})$ represent the propagation constants at angular frequencies ω_P, $\omega_{AS1}=\omega_P+\Omega_1$, and $\omega_{S1}=\omega_P-\Omega_1$ of the initial pump, first anti-Stokes, and first Stokes waves, respectively, and Ω_1 is the first intermodal FWM-induced Stokes frequency shift from the pump wave. Similarly, $\beta^{(2)}(\omega_{AS1})$, $\beta^{(3)}(\omega_{AS2})$, and $\beta^{(3)}(\omega_{S2})$ represent the propagation constants at angular frequencies ω_{AS1}, $\omega_{AS2}=\omega_{AS1}+\Omega_2$, and $\omega_{S2}=\omega_{AS1}-\Omega_2$ of the first anti-Stokes, second anti-Stokes, and second Stokes waves, respectively and Ω_2 is the second intermodal FWM-induced Stokes frequency shift from the first anti-Stokes wave. The superscripts (1), (2), and (3) represent the 1st, 2nd, and 3rd guided-modes of the MPCF. In the calculation, $\delta\beta_{12}$ and $\delta\beta_{23}$ can be derived from the effective refractive indices of the three guided-modes, which can be obtained from Fig. 1(b). Cascaded intermodal FWM process will occur when $\delta\beta_{12}=0$ and $\delta\beta_{23}=0$ are satisfied.

We first calculate $\delta\beta_{12}$ when initial pump pulses at wavelength λ_p = 800 nm and average input power P_{av}=450, 550, and 650 mW (peak powers of 54, 66, and 78 kW) are coupled into the normal dispersion region far away from the ZDW of the 1st guided-mode. From Fig. 3(a), $\delta\beta_{12}$ is zero at the visible and near-infrared wavelengths of 537.8 and 1559.3 nm, respectively. Thus, the first anti-Stokes and Stokes waves propagating in the 2nd guided-mode are generated at these two wavelengths through the first intermodal FWM process. Then the first anti-Stokes wave generated at 537.8 nm serves as the secondary pump for the next intermodal FWM process. Fig. 3(b) shows that the calculated $\delta\beta_{23}$ reaches zero at the shorter UV and near-infrared wavelengths of 376.4 and 944.7 nm, respectively. The second anti-Stokes and Stokes waves are generated in the 3rd guided-mode. Fig. 3(c) shows the whole experimental spectra observed by the two OSAs at the output end of the MPCF. Since femtosecond pump pulses are coupled into the deeply normal dispersion region of the MPCF, both dispersion and self-phase modulation (SPM) govern the initial nonlinear optical process instead of soliton dynamics. From Fig. 3(c), as P_{av} of the initial pump (P) at 800 nm is increased from 450, to 550, and to 650 mW, the first narrowband anti-Stokes (AS1) and Stokes (S1) waves at 538.1 and 1559.5 nm (corresponding to Ω_1 of ~6084 cm^{-1}) are generated. The intensities of the generated AS1 waves are sufficiently strong to serve as the secondary pump for the next intermodal FWM. The second anti-Stokes (AS2) and Stokes (S2) waves are generated at wavelengths 375.8 and 945.4 nm (corresponding to Ω_2 of ~8026 cm^{-1}). From Fig. 3(c), the experimental observations agree well with the calculation results shown in Figs. 3(a) and 3(b). As P_{av} increases, the intensities of the AS1, S1, AS2, and S2 waves are gradually enhanced, but their center wavelengths are kept unchanged.

The observation confirms the assumption that nonlinear contribution to the intermodal phase-matching scheme can be neglected. Such insensitivity to the input power can be utilized to obtain stable-wavelength output signals for commercial applications. Fig. 3(d) shows the zoom-in spectra of the P, AS1, and AS2 waves. Insets 1, 2, and 3 of Fig. 3(d) show the output far-field distributions of the P, AS1, and AS2 waves observed for P_{av}=650 mW, respectively. From the three insets, the P, AS1, and AS2 waves are respectively propagated in the 1st, 2nd, and 3rd guided-modes, which are identical to the spatial distribution profiles calculated for the three guided-modes shown in the insets of Fig. 1(c). The AS1 wave at 538.1 nm and AS2 wave at 375.8 nm are simultaneously generated by the cascaded intermodal FWM process. As shown in Fig. 3(e), for P_{av}=450, 550, and 650 mW at a pump coupling efficiency of 65%, the output powers P_{AS1} and P_{AS2} of the AS1 and AS2 waves, which are measured by the combination of the optical filters and a power meter, are 32.47, 53.63, and 84.92 mW, and 1.76, 4.65, and 10.56 mW, respectively.

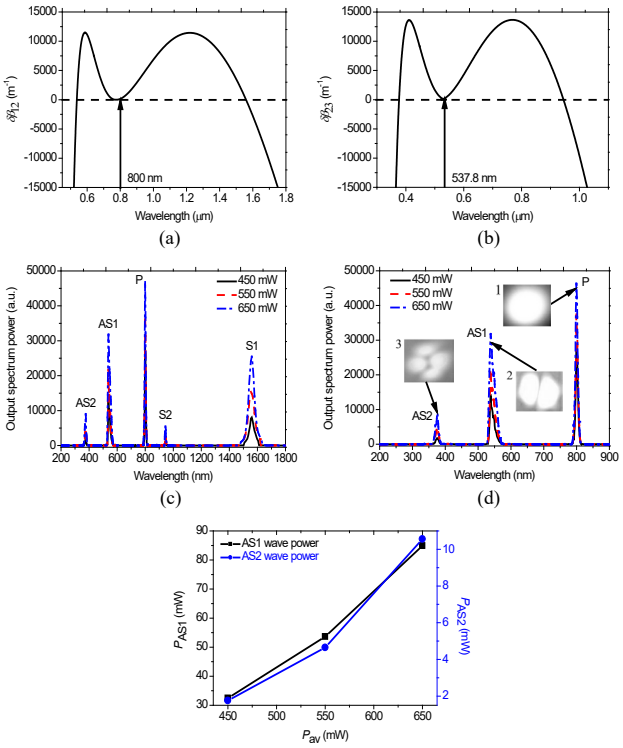

Fig. 3. The phase-mismatch parameters $\delta\beta_{12}$ and $\delta\beta_{23}$ calculated for (a) the first intermodal FWM process and (b) the second intermodal FWM process for initial pump pulses at wavelength λ_p of 800 nm. (c) The observed output spectra including the initial pump (P), first anti-Stokes (AS1), first Stokes (S1), second anti-Stokes (AS2), and second Stokes (S2) waves when the pump pulses at λ_p= 800 nm and average input power P_{av} of 450, 550, and 650 mW (peak powers of 54, 66, and 78 kW) are used. (d) The zoom-in spectra of the P, AS1, and AS2 waves. Insets 1, 2, and 3 show the output far-field distributions of the P, AS1, and AS2 waves recorded by using a black-and-white CCD for P_{av}=650 mW. (e) The dependences of the measured output powers P_{AS1} and P_{AS2} of the AS1 and AS2 waves on P_{av}.

In intermodal nonlinear dynamics, large normal dispersion and SPM together can play an important role in the spectral broadening of the AS1 and AS2 waves propagating in the normal dispersion regions of the 2nd and 3rd guided-modes of the MPCF. The pulse duration of the AS1 wave may be compressed to be shorter than that of the initial pump pulses, resulting in a higher peak power. The energy conversion from the AS1 wave to the AS2 wave could therefore be evidently enhanced. For the S1 and S2 waves located in the anomalous dispersion regions of the 2nd and 3rd guided-modes of the MPCF, soliton-related nonlinear dynamics may occur. In the experiment, we choose a short fiber length, 25 cm, to suppress the multimode SC generation, which is resulted from soliton fission, Raman effect, cross-phase modulation, etc [15,16]. As a result, discrete narrowband spectral components from the UV to near-infrared wavelengths can be obtained.

Next, we investigate the influence of MPCF bending on the cascaded intermodal FWM process. We bend the MPCF by wrapping it around a few cylinders with different diameters. For femtosecond pump pulses at λ_p=800 nm and P_{av}=650 mW, the measured P_{AS1}=84.92 mW and P_{AS2}=10.56 mW. Fig. 4 shows the dependences of P_{AS1} and P_{AS2} on the MPCF bending radius R. From Fig. 4, when R is changed from 20 to 5 mm, P_{AS1} is reduced from 84.92 to 82.09 mW, and P_{AS2} is reduced from 10.56 to 8 mW. The variation rates of P_{AS1} and P_{AS2} with R for the first and second intermodal FWM are only 0.189 and 0.171 mW/mm, respectively. Thus, we concluded that the demonstrated cascaded intermodal FWM-based frequency conversion is not sensitive to MPCF bending. We believe the main reasons are as follows. In general, the near-infrared Stokes waves have significant impact on the unseeded FWM process [11,12]. In the proposed cascaded intermodal FWM, the S1 and S2 waves generated at 1559.5 and 945.4 nm are propagated in the 2nd and 3rd guided-modes, respectively. For the air-silica MPCF used, the d/Λ in the cladding region can be up to 0.89. Thus, the leakage losses of the S1 and S2 waves induced by the fiber bending are effectively suppressed. In addition, the variations of the dispersion and nonlinearity for the 2nd and 3rd guided-modes induced by the MPCF bending can also be neglected.

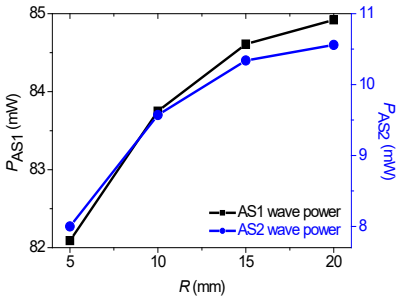

Fig. 4. The output powers P_{AS1} and P_{AS2} of the AS1 and AS2 waves versus the MPCF bending radius R. The pump wavelength λ_p=800 nm, and the average input power P_{av}=650 mW.

Finally, we evaluate the effect of intermodal walk-offs between the guided-modes involved in the FWM process. From [2,14], the intermodal walk-off factors D_{12} between the 1st and 2nd guided-modes and D_{23} between the 2nd and 3rd guided-modes are given as $D_{12}=1/v_g^{(1)}(\lambda)-1/v_g^{(2)}(\lambda)$ and $D_{23}=1/v_g^{(2)}(\lambda)-1/v_g^{(3)}(\lambda)$, where $v_g^{(1)}(\lambda)$, $v_g^{(2)}(\lambda)$, and $v_g^{(3)}(\lambda)$ correspond to the group velocities of the 1st, 2nd, and 3rd guided-modes of the MPCF, respectively. Figs. 5(a) and 5(b) show the variation of the calculated D_{12} and D_{23} with wavelength. From Figs. 5(a) and 5(b), the values of D_{12} and D_{23} are less than 11.5 and 10.8 fs/mm, respectively, from 0.3 to 1.8 μm. D_{12} is ~9.09 fs/mm at λ_p=800 nm and D_{23} is ~8.12 fs/mm at the AS1 wavelength of 538.1 nm. Moreover, because the initial pump pulses are broadened from 120 to 273 fs by the positive-chirp introduced with grating-based compressor, the first intermodal FWM process involved in the P, AS1, and S1 waves can be achieved within a walk-off length of ~3 cm. The second intermodal FWM process involved in the AS1, AS2, and S2 waves can be maintained within a propagation distance of <3.36 cm when we consider that the pulse duration of the AS1 wave generated as the secondary pump could be compressed shorter than the initial pump pulses of 273 fs by the normal dispersion and SPM.

In the proposed cascaded intermodal FWM process, we expected that the AS2 wavelength could be shifted towards the deep-UV spectral

region below 350 nm by optimizing the geometric structures of the MPCF, appropriately choosing the laser pump sources, or combining with other nonlinear optical techniques, such as phase-matched second-harmonics, sum-frequency generation, etc. The output power of the AS2 waves can be enhanced by the following methods. First, we can reduce the leakage and scattering losses of the guided-modes by optimizing the fiber core and cladding structures. We can also minimize the UV absorption loss by using highly purified silica material. Second, the longitudinal non-uniformity and transverse irregularity of the fiber core and cladding structures can be improved during the fiber drawing process in order to alleviate their detrimental effects on the optical field distributions, dispersion characteristics, intermodal phase-matching conditions, and intermodal walk-offs of the three guided-modes considered. Third, intermodal walk-offs can be suppressed by optimizing the MPCF geometric structures (silica-core size and relative air-hole size) and properly adjusting the pump pulse parameters including pulse duration, peak power, and operation wavelength.

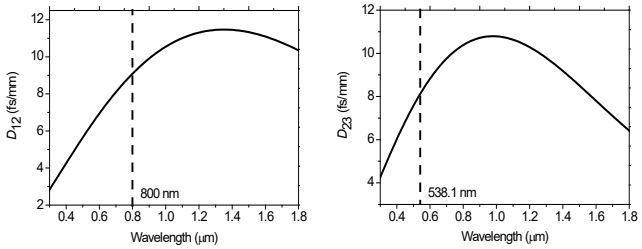

Fig. 5. The calculated intermodal walk-off factors (a) D_{12} and (b) D_{23}. The two vertical dashed lines correspond to the pump wavelength λ_p=800 nm and the AS1 wavelength of 538.1 nm, respectively.

In summary, we have experimentally demonstrated cascaded intermodal FWM-based discrete UV wavelength generation for the first time in a MPCF designed and fabricated in our laboratory. When femtosecond pump pulses at 800 nm are coupled into the deeply normal dispersion region of the 1st guided-mode of the MPCF, intermodal phase-matching between the 1st, 2nd, and 3rd guided-modes can be satisfied. The AS1 waves can be efficiently generated at the visible wavelength of 538.1 nm, which serve as the secondary pump for the next FWM process. Subsequently, the AS2 waves are obtained at the UV wavelength of 375.8 nm. We observed that the cascaded intermodal FWM-based frequency conversion process is insensitive to fiber bending and intermodal walk-offs. We believed the reported findings provide an effective way for the generation of discrete UV wavelengths, which can be used as the UV light source and would be of immediate interest in applications such as biomedical science, fluorescence spectroscopy.

Funding sources and acknowledgments. National Natural Science Foundation of China (61475023), the Beijing Youth Top-notch Talent Support Program (2015000026833ZK08), the Beijing Natural Science Foundation (4152037), the Fund of State Key Laboratory of Information Photonics and Optical Communications (BUPT) P. R. China (IPOC2016ZT05), and the Research Grant Council of the Hong Kong SAR China (PolyU152173/17E).

References

[1] P. St. J. Russell, P. Hölzer, W. Chang, A. Abdolvand and J. C. Travers, Nat. Photonics **8**, 278 (2014).
[2] F. Poletti, and P. Horak, Opt. Express **17**, 6134 (2009).
[3] A. C. Peacock, P. Mehta, P. Horak, and N. Healy, Opt. Lett. **37**, 3351 (2012).
[4] A. Mafi, J. Lightw. Technol. **30**, 2803 (2012).
[5] L. G. Wright, D. N. Christodoulides, and F. W. Wise, Nat. Photonics **9**, 306 (2015).
[6] Y. Yang, X. F. Jiang, S. Kasumie, G. M. Zhao, L. H. Xu, J. M. Ward, L. Yang, and S. N. Chormaic, Opt. Lett. **41**, 5266 (2016).
[7] W. H. Renninger, and F. W. Wise, Nat. Commun. **4**, 1719 (2013).
[8] S. Buch, and G. P. Agrawal, Opt. Lett. **40**, 225 (2015).
[9] A. Tonello, S. Pitois, S. Wabnitz, G. Millot, T. Martynkien, W. Urbanczyk, J. Wojcik, A. Locatelli, M. Conforti, and C. De Angelis, Opt. Express **14**, 397 (2006).
[10] C. Lesvigne, V. Couderc, A. Tonello, P. Leproux, A. Barthélémy, S. Lacroix, F. Druon, P. Blandin, M. Hanna, and P. Georges, Opt. Lett. **32**, 2173 (2007).
[11] H. Tu, Z. Jiang, D. L. Marks, and S. A. Boppart, Appl. Phys. Lett. **94**, 101109 (2009).
[12] J. H. Yuan, X. Z. Sang, Q. Wu, G. Y. Zhou, F. Li, X. Zhou, C. X. Yu, K. R. Wang, B. B. Yan, Y. Han, H. Y. Tam, and P. K. A. Wai, Opt. Lett. **40**, 1338 (2015).
[13] R. Dupiol, A. Bendahmane, K. Krupa, A. Tonello, M. Fabert, B. Kibler, T. Sylvestre, A. Barthelemy, V. Couderc, S. Wabnitz, and G. Millot, Opt. Lett. **42**, 1293 (2017).
[14] G. P. Agrawal, Nonlinear Fiber Optics (Academic, 2013).
[15] J. M. Dudley, G. Genty, and S. Coen, Rev. Mod. Phys. **78**, 1135 (2006).
[16] J. M. Dudley, and J. R. Taylor, Nat. Photonics **3**, 85 (2009).

References

[1] P. St. J. Russell, P. Hölzer, W. Chang, A. Abdolvand and J. C. Travers, "Hollow-core photonic crystal fibres for gas-based nonlinear optics," Nat. Photonics, vol.8, pp.278-286, 2014.

[2] F. Poletti, and P. Horak, "Dynamics of femtosecond supercontinuum generation in multimode fibers," Opt. Express, vol.17, pp.6134-6147, 2009.

[3] A. C. Peacock, P. Mehta, P. Horak, and N. Healy, "Nonlinear pulse dynamics in multimode silicon core optical fibers," Opt. Lett., vol.37, pp.3351-3353, 2012.

[4] A. Mafi, "Pulse propagation in a short nonlinear graded-index multimode optical fiber," J. Lightw. Technol., vol.30, pp.2803-2811, 2012.

[5] L. G. Wright, D. N. Christodoulides, and F. W. Wise, "Controllable spatiotemporal nonlinear effects in multimode fibres," Nat. Photonics, vol.9, pp.306-310, 2015.

[6] Y. Yang, X. F. Jiang, S. Kasumie, G. M. Zhao, L. H. Xu, J. M. Ward, L. Yang, and S. N. Chormaic, "Four-wave mixing parametric oscillation and frequency comb generation at visible wavelengths in a silica microbubble resonator," Opt. Lett., vol.41, pp.5266-5269, 2016.

[7] W. H. Renninger, and F. W. Wise, "Optical solitons in graded-index multimode fibres," Nat. Commun., vol.4, pp.1719-1-6, 2013.

[8] S. Buch, and G. P. Agrawal, "Soliton stability and trapping in multimode fibers," Opt. Lett., vol.40, pp.225-228, 2015.

[9] A. Tonello, S. Pitois, S. Wabnitz, G. Millot, T. Martynkien, W. Urbanczyk, J. Wojcik, A. Locatelli, M. Conforti, and C. De Angelis, "Frequency tunable polarization and intermodal modulation instability in high birefringence holey fiber," Opt. Express, vol.14, pp.397-404, 2006.

[10] C. Lesvigne, V. Couderc, A. Tonello, P. Leproux, A. Barthélémy, S. Lacroix, F. Druon, P. Blandin, M. Hanna, and P. Georges, "Visible supercontinuum generation controlled by intermodal four-wave mixing in microstructured fiber," Opt. Lett., vol.32, pp.2173-2175, 2007.

[11] H. Tu, Z. Jiang, D. L. Marks, and S. A. Boppart, "Intermodal four-wave mixing from femtosecond pulse-pumped photonic crystal fiber," Appl. Phys. Lett., vol.94, pp.101109-1-3, 2009.

[12] J. H. Yuan, X. Z. Sang, Q. Wu, G. Y. Zhou, F. Li, X. Zhou, C. X. Yu, K. R. Wang, B. B. Yan, Y. Han, H. Y. Tam, and P. K. A. Wai, "Enhanced intermodal four-wave mixing for visible and near-infrared wavelength generation in a photonic crystal fiber," Opt. Lett., vol.40, pp.1338-1341, 2015.

[13] R. Dupiol, A. Bendahmane, K. Krupa, A. Tonello, M. Fabert, B. Kibler, T. Sylvestre, A. Barthelemy, V. Couderc, S. Wabnitz, and G. Millot, "Far-detuned cascaded intermodal four-wave mixing in a multimode fiber," Opt. Lett., vol.42, pp.1293-1296, 2017.

[14] G. P. Agrawal, Nonlinear Fiber Optics (Academic, 2013).

[15] J. M. Dudley, G. Genty, and S. Coen, "Supercontinuum generation in photonic crystal fiber," Rev. Mod. Phys., vol.78, pp.1135-1184, 2006.

[16] J. M. Dudley, and J. R. Taylor, "Ten years of nonlinear optics in photonic crystal fibre," Nat. Photonics, vol.3, pp.85-90, 2009.